IEEE Access
Multidisciplinary ⋮ Rapid Review ⋮ Open Access Journal

Received 27 March 2023, accepted 12 April 2023, date of publication 21 April 2023, date of current version 26 April 2023.

Digital Object Identifier 10.1109/ACCESS.2023.3269285

RESEARCH ARTICLE

Passive IR-UWB Localization System for UAV-Based Electric Facility Inspection During GPS Outage

UI-SUK SUH[1,2], GEUNHAENG LEE[3], JIEUN HAN[1], TAE WOOK KIM[2], (Senior Member, IEEE), AND WON-SANG RA[1]

[1]Department of Mechanical and Control Engineering, Handong Global University, Pohang 37554, South Korea
[2]Department of Electrical and Electronic Engineering, Yonsei University, Seoul 03722, South Korea
[3]Department of Electronic Engineering, Andong National University, Andong 36729, South Korea

Corresponding author: Won-Sang Ra (wonsang@handong.edu)

This work was supported in part by the Korea Institute of Energy Technology Evaluation and Planning (KETEP) and the Ministry of Trade, Industry & Energy (MOTIE) of the Republic of Korea (No. 20214000000010) and in part by the Ministry of Science and ICT (2014M1A3A3A02034806; Geunhaeng Lee performed this work during his Ph.D. studies at Yonsei University).

ABSTRACT A practical localization system is proposed for an unmanned aerial vehicle (UAV) performing its inspection mission under the global positioning system (GPS) signal blockage. The sensor hardware consists of a single transmitter and a cruciform receiver array, which produces the range difference (RD) information for UAV positioning. Our sensor is based on the impulse-radio ultra wide-band (IR-UWB) technology; hence it is robust to RF interference due to exogeneous electromagnetic fields from electric facilities. With this sensor configuration, UAV localization problem is formulated as state estimation for an uncertain linear measurement model, which can be solved by using the robust weighted least squares (RWLS) estimator. To cope with the performance degradation of the RWLS estimator due to the imperfect prior knowledge of the measurement noise statistics, a geometric constraint expressed by the UAV state variables is exploited to compensate the localization errors. Through experimental results, it is verified that the proposed solution provides satisfactory UAV positioning performance and secures the reliability of the localization system in practice.

INDEX TERMS Substation inspection, UAV positioning system, IR-UWB transceivers, constrained estimation.

I. INTRODUCTION

An electric substation that supplies electrical power to consumers is one of the most critical facilities in power grids. Failures of substation components may lead to severe accidents such as fires, explosions, and blackouts. To prevent power grids from accidents, it is crucial to inspect the substation periodically [1], [2], [3]. However, it is a daunting or even dangerous task to inspect all the substation components in person. Since many components are widely distributed across a substation site, much time and effort are required for their health check. Moreover, human inspectors could be exposed to unsafe working conditions due to high-voltage or high-current environments of the substation. As a practical resolution to these problems, an autonomous inspection system based on unmanned aerial vehicles (UAVs) with portable diagnosis devices has been studied recently [3].

Existing inspection UAVs analyze the failure risks by following a planned flight path around the electric facilities of interest [4], [5]. They assume that the UA,s position is always available from a global positioning system (GPS) for flight control. However, as shown in Fig. 1, when the UAV flies underneath or near the facilities, the GPS signal could be blocked by the complicated metal structures of the substation [6]. Besides, an electromagnetic field formed around high-voltage transmission lines may cause unpredictable

The associate editor coordinating the review of this manuscript and approving it for publication was Min Wang.

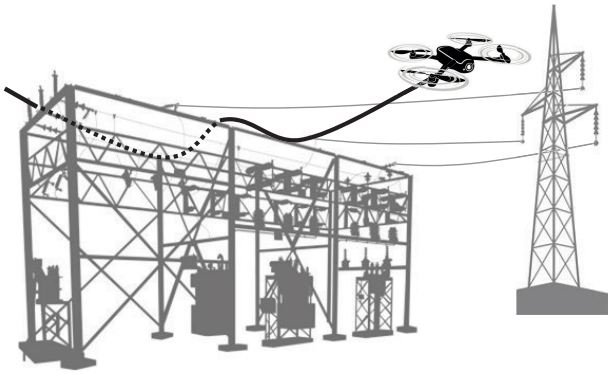

FIGURE 1. Substation inspection UAV at GPS-denied environment.

navigation errors of the GPS [7]. Therefore, a new localization system is crucial for a UAV to accomplish its inspection mission under GPS-denied environments.

To tackle this technical issue, vision-based simultaneous localization and mapping (SLAM) has been attempted by many researchers [8], [9]. By applying a nonlinear Kalman filter to the image data acquired from the vision sensor, this approach tries to detect the prescribed electric facilities, construct an environmental map, and localize a UAV ultimately. Despite remarkable theoretical advances, the vision-based SLAM could fail to guarantee reliable UAV positioning in practice. Since the UAV localization performance of this method is influenced by the image quality, it tends to be susceptible to motion blur or variations in weather conditions [10]. In addition, their application might be restrictive because of the heavy computational burden of image processing [11].

On the other hand, a wireless communication-based localization system was suggested for UAV localization [12], [13], [14]. The underlying idea of this approach is to estimate the position of an inspection UAV by using the range information between the UAV and the transceivers attached to the region where the GPS signal blockage often occurs. Based on this concept, a UAV localization system using onboard ultrasonic range finders was developed [12]. Through prior knowledge of the beam pattern model of the ultrasonic arrays, this system tried to enhance both the range measurement accuracy and the UAV localization performance. However, its performance could be severely deteriorated due to the multi-path, which makes this methodology inapplicable.

To supplement this shortcoming of the previous wireless communication-based positioning systems, the impulse radio ultra-wideband (IR-UWB) technology was applied [13], [14], [15]. It can drastically reduce multi-path and delay caused by signal interference or reflection [13]. Most IR-UWB localization systems use synchronized transceivers to obtain the distance of a UAV to the reference position. Therefore, this approach is not an affordable solution because an expensive synchronizer is needed to interlock the transceivers for enhanced accuracy of distance measurements [16]. Furthermore, this methodology usually utilizes nonlinear filters to estimate the UAV position using a set of distance measurements; hence it is unsuitable for real-time implementation on a cheap microprocessor [17].

To overcome these flaws, this paper proposes a novel IR-UWB localization system shown in Fig. 2. The proposed system consists of passive sensors which measure the range difference (RD) using IR-UWB transceivers. The RD measuring sensor consists of a transmitter placed at a region of GPS signal blockage and a cruciform receiver array mounted on the UAV. Due to the passive manner of RD measuring, our sensor does not require an expensive synchronization device. Thus, unlike the previous IR-UWB distance measuring scheme, our RD measuring device is cost-effective. Meanwhile, for computational efficiency, the UAV localization problem is solved within the framework of a linear robust state estimation theory. To do this, the nonlinear relationship between the RD measurement and the relative UAV position is first modeled as an uncertain linear measurement equation. Then, a UAV localization algorithm is designed by applying the robust weighted least-squares (RWLS) estimation theory to the measurement model [18]. Provided that the statistical knowledge on the RD measurement is perfectly known, the RWLS estimator guarantees the unbiasedness, and the fast convergence of the UAV position estimates. However, this is not the case in real applications where the exact statistical knowledge of the RD measurement is unavailable. To secure the reliability of UAV positioning, a constrained RWLS (C-RWLS) localization algorithm is designed. Noticing that the imperfect measurement noise statistics result in the unwanted scale-factor error of the design parameter used for the RWLS estimator, the correct design parameter is calculated by using the equality constraint about the geometric relationship among the UAV state estimates. Accordingly, our C-RWS localization algorithm enables precise UAV positioning even when the statistical property of the measurement noise is uncertain. To check the validity of the proposed UAV localization system, an RD measuring sensor is implemented using an IR-UWB transceiver chipset, and its localization performance is analyzed through experiments.

II. IR-UWB RANGE DIFFERENCE SENSOR DESIGN

A. SYSTEM CONFIGURATION

This section briefly introduces the configuration of the proposed localization system for the substation inspection UAV. As shown in Fig. 2, the proposed system consists of a range difference (RD) measuring sensor, and a localization algorithm embedded in the digital signal processor (DSP) that estimates the relative UAV position. The RD measuring sensor is comprised of an impulse radio ultra-wideband (IR-UWB) transmitter located at a known position and five cruciform receiver arrays mounted on the UAV. Since the receivers Rx #j in Fig. 2 are spaced equally from the reference Rx #0 by width d, the RD can be defined as the Δt_j between the received time difference of arrivals (TDOAs) from Rx #0 and its neighboring Rx #j.

$$\Delta t_j \triangleq t_j - t_0, \quad j = 1, 2, \cdots, 4. \tag{1}$$

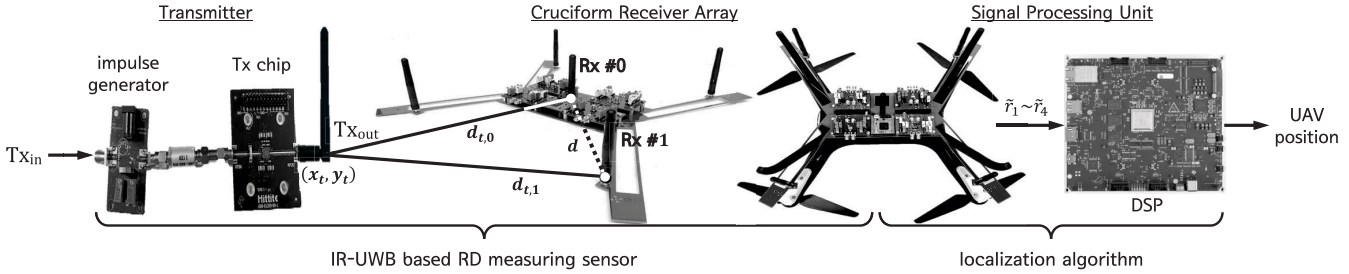

FIGURE 2. Configuration of the proposed localization system.

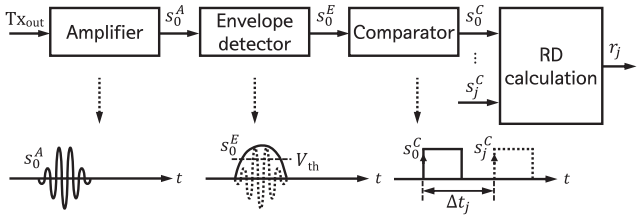

FIGURE 3. Signal processing unit of receiver array.

Then, the RD r_j is easily derived by multiplying (1) with the speed of light c as follows:

$$r_j \triangleq c \cdot \Delta t_j, \quad c = 3 \cdot 10^8 \text{ [m/s]}. \tag{2}$$

Fig. 3 is the signal processing unit of the RD measuring sensor. When a transmitter generates an impulse, each receiver detects and amplifies the magnitude of the received signal. Also, an envelope detector is developed to be self-mixing to improve the detection efficiency to pick the outside of the signal. Next, a comparator converts the envelope signal to pulse by comparing the envelope and the preset threshold, V_{th}. Finally, the RD information r_j is calculated by TDOA Δt_j between the rising edges s_0^C and s_j^C.

B. ERROR ANALYSIS OF RANGE DIFFERENCE MEASUREMENT

The RD information obtained from the devised IR-UWB transceivers inevitably includes measurement noise. It is well-known that the Gaussian thermal noise of the receiver is the most apparent component of the noises [19]. The thermal noise can convert into jitter at the rising edge of the receiver output, which results in RD output errors. Thus, the RD measurement $\tilde{r}_j$ is expressed as the summation of the true RD r_j and its measurement noise δr_j following a Gaussian distribution as follows:

$$\tilde{r}_j = r_j + \delta r_j, \quad \delta r_j \sim \mathcal{N}(0, \sigma_{r,j}^2), \tag{3}$$

where $\sigma_{r,j}^2$ is the variance of the RD measurement $\tilde{r}_j$.

Remark 1: The walk error and time variation also correspond to a minor bias error in the RD measurement [20]. Walk errors are a type of delayed effect. If the amplitude of the envelope signal decreases as the measured distance increases, the digital signal generated will be delayed in the analog comparator. Also, the timing error due to the gain deviation between receivers can be regarded as a time variation.

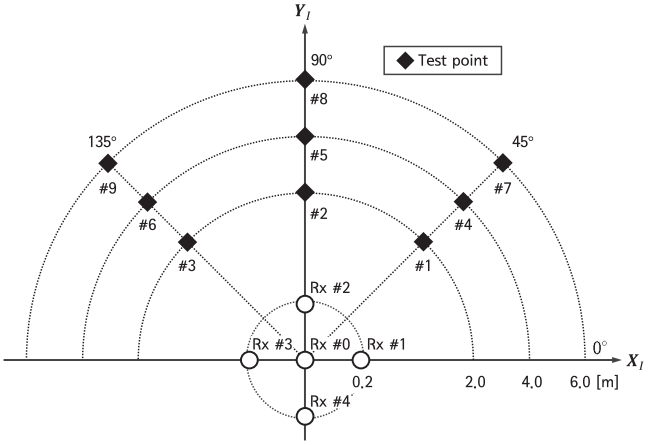

FIGURE 4. Test points.

Remark 2: The walk error mentioned in ***Remark 1*** is deterministic, so it can be easily removed using batch calibration. Then, the gain variation is compensated with the individual calibration method [21]. Thus, the error of the RD measurement obtained from the devised sensor can be modeled as Gaussian thermal noise, as shown in (3).

C. RESULT OF RANGE DIFFERENCE MEASUREMENT

The measurement error properties of our RD sensor are analyzed through experiments. As illustrated in Fig. 4, various transmitter locations are set to confirm the performance of the receiver array. The system configuration of our sensor is shown in Fig. 2. The signal generator excites the clock Tx_{in} to the transmitter, and the received signal outputs a digital pulse s_j^C from each receiver chipset. Afterward, s_j^C is measured using a multi-channel oscilloscope. The receiving antennas are arranged in a cruciform with a spacing of $d = 0.2$[m]. In the measurement setup, an omni-directional monopole antenna with 0[dBi] antenna gain is used, and the receivers, which were fabricated with 65[nm] CMOS, are mounted on a printed circuit board (PCB) using the chip-on-board (COB) technique. The devised receiver consumes 50[mA] with 1.2[V] supply voltage.

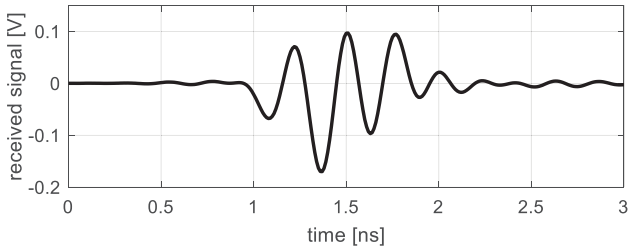

FIGURE 5. Received IR-UWB signal.

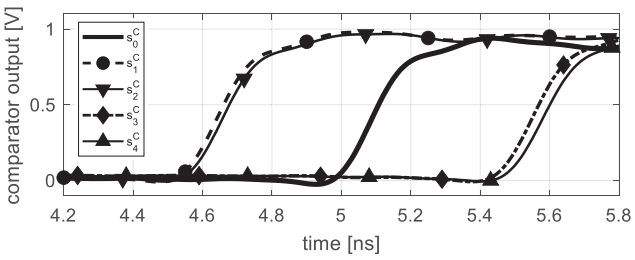

FIGURE 6. Comparator output.

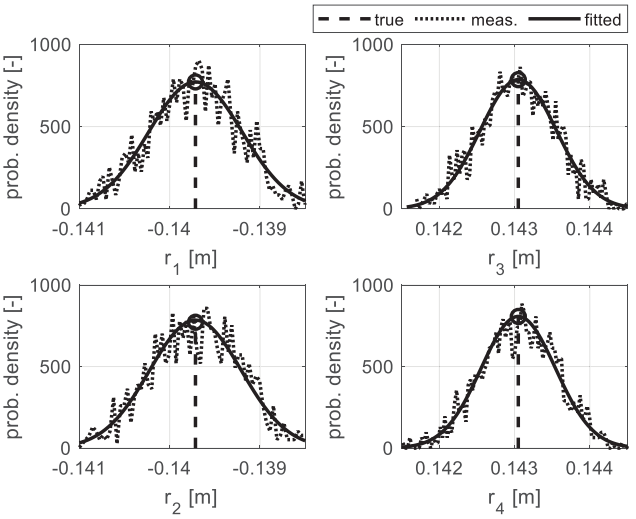

FIGURE 7. Error modeling of RD measurements.

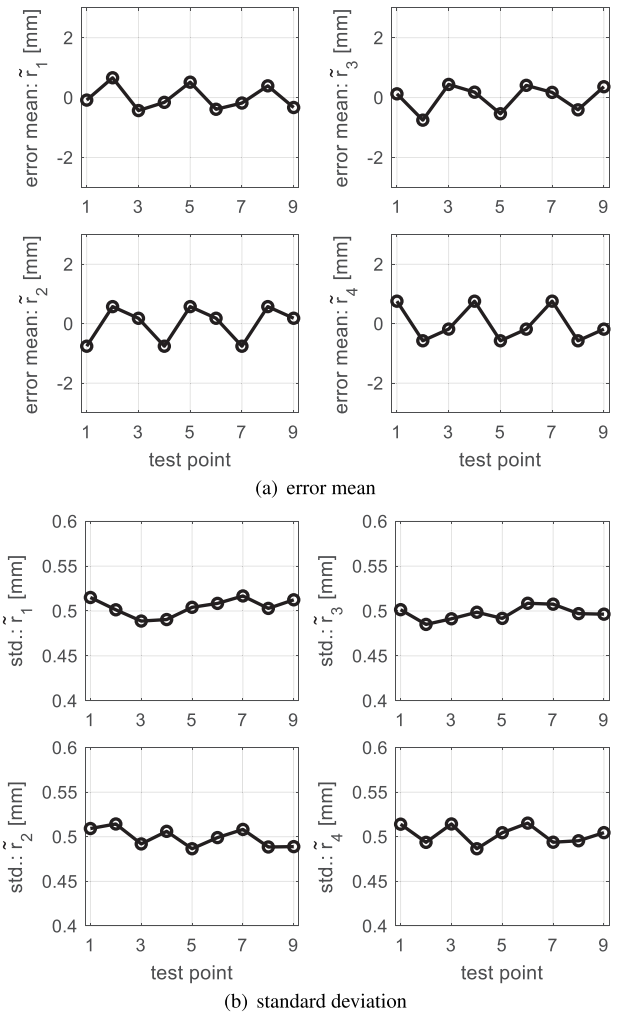

FIGURE 8. Statistical characteristics of RD measurements.

Using the transceivers described above, the measured received impulse waveform at the reference receiver Rx #0 is depicted in Fig. 5 when the transmitter is placed in point #7 in Fig. 4. From this result, it is confirmed that this signal has a maximum amplitude of 0.25[V_{pp}]. Then, the above impulse is converted to a digital pulse in the receiver, and its pulse waves are captured using an oscilloscope. At this time, the TDOA is measured between an output pulse, which is transformed from the envelope of the received impulse of the reference, and that of an adjacent receiver. The measured pulses are shown in Fig. 6. It can be seen that all the received pulses have almost identical rising slopes. It implies that our RD measuring sensor can obtain precise RD measurements.

Next, the receiver array is reviewed to observe whether it provides precise RD measurements. Fig. 7 is the histogram of the 1000 RD measurement samples at test point #7 in Fig. 4 and its fitted result. The obtained RD measurements have a Gaussian distribution with a mean value close to the true RD information. In addition, as mentioned in Section II-B, the measurement noise of the proposed RD measuring sensor mainly includes Gaussian thermal noise. Therefore, it is possible to model the statistical properties of the measured values with a Gaussian distribution like the fitted results (solid line in Fig.7).

Based on the above analysis, the RD measurement is regarded as Gaussian distribution. So, the statistical properties of the RD measurements at all the test points in Fig. 4 are described as the error mean and standard deviation of the measurement noise depicted in Fig. 8. The overall RD measurements nearly maintain zero mean and standard deviation of approximately 0.5[*m*m]. Note that minor bias depending on the range, such as walk errors, can be easily removed through batch calibration, as described in ***Remark 2***. In summary, the devised RD measuring sensor is able to provide a precise RD measurement, as shown in the experiments.

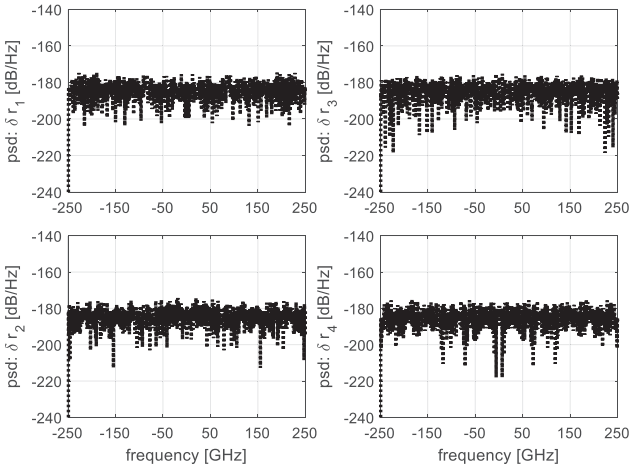

FIGURE 9. PSD of RD measurement error.

Remark 3: The proposed localization algorithm in Section III assumes that the RD measurement noise is white. It means that the RD measurement noise does not have to follow the Gaussian distribution, as shown in Fig. 7. The power spectral density (PSD) of the noise in Fig. 7 is shown in Fig. 9, and it can be seen that all RD noise satisfies the white noise condition. To summarize, it is possible to design our localization estimator obtained from the devised sensor.

Remark 4: Even if the RD measurements are contaminated by colored noises, the well-known pre-whitening filter can be applied to the raw measurements [22], [23]. In this case, the design requirement of our localization algorithm can be met.

III. ROBUST LINEAR LOCALIZATION APPROACH USING RANGE DIFFERENCE MEASUREMENTS

In this section, a UAV localization algorithm is designed using RD measurements obtained from the sensor devised in the previous section.

A. UNCERTAIN LINEAR MEASUREMENT MODEL

To solve the UAV localization problem within the framework of linear state estimation theory, let us derive the relationship between the RD measurement and the relative position of the inspection UAV as an uncertain linear state-space model. From Fig. 2, the RD r_j is defined as follows:

$$r_j \triangleq d_{t,j} - d_{t,0}, \quad j = 1, 2, \cdots, 4. \tag{4}$$

In the above equation, the distance from the transmitter to the jth receiver $d_{t,j}$ is given by (5).

$$d_{t,j} = \sqrt{(x_t - x_j)^2 + (y_t - y_j)^2} \tag{5}$$

Using a similar method to (5), the distance from the reference receiver to the jth receiver $d_{j,0}$ can be written as

$$d_{j,0} = \sqrt{(x_j - x_0)^2 + (y_j - y_0)^2}. \tag{6}$$

After squaring both sides of (4) and inserting (5), we have

$$r_j^2 - d_{j,0}^2 = h_j \begin{bmatrix} x_t - x_0 \\ y_t - y_0 \\ d_{t,0} \end{bmatrix}, \quad h_j = -2 \begin{bmatrix} x_j - x_0 \\ y_j - y_0 \\ r_j \end{bmatrix}. \tag{7}$$

Substituting (3) for (7) results in an uncertain linear measurement equation (8).

$$\tilde{r}_j^2 - d_{j,0}^2 - \sigma_{r_j}^2 = \left[\tilde{h}_j - \Delta h_j\right] \begin{bmatrix} x_t - x_0 \\ y_t - y_0 \\ d_{t,0} \end{bmatrix} + v_j, \tag{8}$$

where

$$\tilde{h}_j \triangleq -2\left[(x_j - x_0) \ (y_j - y_0) \ \tilde{r}_j\right],$$
$$\Delta h_j \triangleq -2\left[0 \ 0 \ \delta r_j\right], \quad v_j \triangleq 2\tilde{r}_j \delta r_j - \delta r_j^2 - \sigma_{r_j}^2.$$

The noise variance of the above measurement model R_j can be calculated as follows:

$$R_j \triangleq var\left\{v_j\right\} = 2\sigma_{r_j}^2 \left(2r_j^2 + \sigma_{r_j}^2\right). \tag{9}$$

Because the equation (8) holds for all receivers, at time instant k, we can define the following uncertain linear measurement model.

$$\boldsymbol{y}_k = H_k \boldsymbol{x}_k + \boldsymbol{v}_k = \left[\tilde{H}_k - \Delta H_k\right] \boldsymbol{x}_k + \boldsymbol{v}_k \tag{10}$$

In the above equation, the state vector $\boldsymbol{x}$, the measurement vector $\boldsymbol{y}$, the measurement noise vector $\boldsymbol{v}$, and the matrices are defined as follows:

$$\boldsymbol{x} \triangleq \begin{bmatrix} x_t - x_0 \\ y_t - y_0 \\ d_{t,0} \end{bmatrix}, \boldsymbol{y} \triangleq \begin{bmatrix} \vdots \\ \tilde{r}_j^2 - d_{j,0}^2 - \sigma_{r_j}^2 \\ \vdots \end{bmatrix}, \ \boldsymbol{v} \triangleq \begin{bmatrix} \vdots \\ v_j \\ \vdots \end{bmatrix},$$

$$H \triangleq \begin{bmatrix} \vdots \\ h_j \\ \vdots \end{bmatrix}, \ \tilde{H} \triangleq \begin{bmatrix} \vdots \\ \tilde{h}_j \\ \vdots \end{bmatrix}, \ \Delta H \triangleq \begin{bmatrix} \vdots \\ \Delta h_j \\ \vdots \end{bmatrix}.$$

Note that the matrix $\tilde{H}_k$ in (10) can be constructed by the RD measurements and is available for UAV localization. This matrix is decomposed into the noise-free observation matrix H_k, which is not known in real cases, and the stochastic parametric uncertainty matrix ΔH_k.

$$\tilde{H}_k = H_k + \Delta H_k \tag{11}$$

Using (9) and (10), the following statistical properties of ΔH_k and $\boldsymbol{v}_k$ are obtained.

$$E\left\{\boldsymbol{v}_k\right\} = 0^{4\times 1}, \quad E\left\{\Delta H_k\right\} = 0^{4\times 3} \tag{12}$$

$$R_k \triangleq var\left\{\boldsymbol{v}_k\right\} = diag\left(\left[\cdots R_j \cdots\right]\right) \tag{13}$$

$$W_k \triangleq E\left\{\Delta H_k^T R_k^{-1} \Delta H_k\right\} = diag\left(\begin{bmatrix} 0 & 0 & \sum_{j=1}^{4} \frac{2}{2r_j^2 + \sigma_{r_j}^2} \end{bmatrix}\right) \tag{14}$$

$$V_k \triangleq E\left\{\Delta {H_k}^T {R_k}^{-1} \boldsymbol{v}_k\right\} = \begin{bmatrix} 0 & 0 & \sum_{j=1}^{4} \frac{2r_j}{2{r_j}^2 + {\sigma_{r_j}}^2} \end{bmatrix}^T \tag{15}$$

TABLE 1. Robust weighted least-squares method [18].

∗ Measurement model

$$\boldsymbol{y}_k = [\tilde{H}_k - \Delta H_k]\boldsymbol{x}_k + \boldsymbol{v}_k$$

∗ Known statistics

$$E\{\boldsymbol{v}_k\} = \mathbf{0}, \quad E\{\Delta H_k\} = \mathbf{0},$$
$$W_k = E\left\{\Delta H_k^T R_k^{-1} \Delta H_k\right\}, \quad V_k = E\left\{\Delta H_k^T R_k^{-1} \boldsymbol{v}_k\right\}$$

∗ Estimate

$$(P_k)^{-1} = \sum_{i=0}^{k} \left\{(\tilde{H}_i)^T R_i^{-1} \tilde{H}_i - W_i\right\}$$
$$\hat{\boldsymbol{x}}_k = P_k \sum_{i=0}^{k} \left\{(\tilde{H}_i)^T R_i^{-1} \mathbf{y}_i - V_i\right\}$$

Remark 5: The devised RD measuring sensor equips the five identical receivers which are arranged in a cruciform structure and are placed with equi-distance d from the reference receiver Rx #0. Hence, it is assumed that the variances in the RD measurement noise are nearly equal to each other. As shown in Fig. 8b, the variances of the RD measurement noise at various test points have almost similar values. This implies that the experimental results support the above assumption. That is, $\sigma_{r,j}^2 \approx \sigma_r^2$, thus (15) can be approximated as follows:

$$V_k \approx 0^{3\times 1}. \tag{16}$$

B. CONSTRAINED ROBUST WEIGHTED LEAST-SQUARES LOCALIZATION ALGORITHM

To effectively solve the localization problem with an uncertain measurement model, the robust weighted least-squares (RWLS) estimation theory summarized in TABLE 1 is considered [18]. The RWLS algorithm adopts the estimation design parameters W_k and V_k to remove the estimation errors caused by the parametric uncertainty ΔH_k. To obtain satisfactory RWLS-based localization performance, a standing assumption about using precise design parameters is required. Unfortunately, if the *a priori* statistical properties of the RD measurement σ_r^2 are not exact, the design parameter cannot be calculated correctly, which may lead to performance degradation.

This issue can be tackled by the constrained RWLS (C-RWLS) in ***Theorem 1*** and ***Theorem 2***.

Theorem 1: **(C-RWLS estimator for UAV localization)** The UAV position estimate is calculated by the C-RWLS estimator.

$$(P_k^c)^{-1} = \sum_{i=0}^{k} \left\{(\tilde{H}_i)^T R_i^{-1} \tilde{H}_i\right\} - (1+\gamma) W_i \tag{17}$$

$$\hat{\boldsymbol{x}}_k^c = P_k^c \sum_{i=0}^{k} \left\{(\tilde{H}_i)^T R_i^{-1} \mathbf{y}_i\right\} \tag{18}$$

In (17), γ denotes an imperfectness of the available design parameter W.

□

proof: Recall that the design parameter W is determined by the prior knowledge about the RD measurement noise statistics as shown in (14). For the sake of convenience, W can be rewritten as follows:

$$W = diag\left(\begin{bmatrix}0 & 0 & w\end{bmatrix}\right), \quad w = \sum_{j=1}^{4} \frac{2\sigma_j^2}{R_j}. \tag{19}$$

Noticing that W is a sparse matrix, we can simply compensate its imperfectness by introducing a scalar constant γ. That is, the perfect but unavailable design parameter W^o can be rewritten as

$$W^o = (1+\gamma) W. \tag{20}$$

In (20), γ represents the scale-factor error of the available design parameter W.

By substituting W^o in (20) into W of the RWLS estimator in TABLE 1, the C-RWLS estimator can be easily derived.

■

In order to implement the C-RWLS estimator in ***Theorem 1***, we should devise an algorithm to calculate the scale-factor error γ.

To do this, let us consider the estimates $\hat{\boldsymbol{x}}_k^o$ and $\hat{\boldsymbol{x}}_k$, which are calculated using the perfect and imperfect design parameter W^o and W, respectively.

$$(P_k^o)^{-1} = \sum_{i=0}^{k} \left\{(\tilde{H}_i)^T R_i^{-1} \tilde{H}_i\right\} - W_i^o,$$
$$\hat{\boldsymbol{x}}_k^o = P_k^o \sum_{i=0}^{k} \left\{(\tilde{H}_i)^T R_i^{-1} \mathbf{y}_i\right\}, \tag{21}$$

and

$$(P_k)^{-1} = \sum_{i=0}^{k} \left\{(\tilde{H}_i)^T R_i^{-1} \tilde{H}_i\right\} - W_i,$$
$$\hat{\boldsymbol{x}}_k = P_k \sum_{i=0}^{k} \left\{(\tilde{H}_i)^T R_i^{-1} \mathbf{y}_i\right\}. \tag{22}$$

Inserting (20) into (21) and rearranging the results, the ideal RWLS estimate $\hat{\boldsymbol{x}}^o$ calculated using the perfect design parameter W^o can be rewritten as a function of the imperfect design parameter W and the nominal RWLS estimate $\hat{\boldsymbol{x}}$.

$$\hat{\boldsymbol{x}}_k^o = (I - \gamma k P_k W)^{-1} \hat{\boldsymbol{x}}_k \tag{23}$$

From the definition of the state variables $\boldsymbol{x}$ in (10), the following hard constraint is derived.

$$(x_t - x_0)^2 + (y_t - y_0)^2 - d_{t,0}^2 = 0 \rightarrow \boldsymbol{x}^T M \boldsymbol{x} = 0 \tag{24}$$

In (24), the weighting matrix M is defined as

$$M \triangleq diag\left(\begin{bmatrix}1 & 1 & -1\end{bmatrix}\right).$$

TABLE 2. Configuration of experiment environment.

ITEM	CONTENT
UAV	∗ Product name: HUINS Blueeye-1k
	∗ Height : $h = 0.88$ [m]
Acquisition for true data	OptiTrack (precise indoor localization system)

Note that (24) indicates the geometric constraint among the state variables $\boldsymbol{x}$. It is well-known that the ideal RWLS estimate $\hat{\boldsymbol{x}}_k^o$ almost surely converges to the true state variable $\hat{\boldsymbol{x}}_k$; hence it also satisfies the constraint (24). Using this property, the unknown constant γ, which compensates the scale-factor error of W, can be calculated.

Theorem 2: **(Calculating the scale-factor error of the design parameter)** The constraint condition (24) can be transformed into a quadratic equation of λ.

$$c(\lambda) = \sum_{m=0}^{2} c_m \lambda^m = 0, \quad \lambda \triangleq \frac{\gamma k}{1 - \gamma k w p_{33}}, \tag{25}$$

where

$$\begin{aligned} c_0 &= \hat{\boldsymbol{x}}_k^T M \hat{\boldsymbol{x}}_k, \\ c_1 &= \hat{\boldsymbol{x}}_k^T (M P_k W_k + W_k P_k M) \hat{\boldsymbol{x}}_k, \\ c_2 &= \hat{\boldsymbol{x}}_k^T (W_k P_k M P_k W_k) \hat{\boldsymbol{x}}_k, \\ P_k &\triangleq \begin{bmatrix} p_{11} & p_{12} & p_{13} \\ * & p_{22} & p_{23} \\ * & * & p_{33} \end{bmatrix}. \end{aligned}$$

By solving (25), the scale-factor error γ can be obtained. □

proof: The ideal RWLS estimate $\hat{\boldsymbol{x}}^o$ in (23) is substituted into the geometric constraint (24).

$$\hat{\boldsymbol{x}}_k^T (I - \gamma k P_k W)^{-T} M (I - \gamma k P_k W)^{-1} \hat{\boldsymbol{x}}_k = 0 \tag{26}$$

The matrix $(I - \gamma k P_k W)$ can be diagonalized as follows:

$$I - \gamma k P_k W = S D S^{-1}, \tag{27}$$

where

$$S = \begin{bmatrix} 1 & 0 & p_{13}/p_{33} \\ 0 & 1 & p_{23}/p_{33} \\ 0 & 0 & 1 \end{bmatrix}, \quad D = I - \gamma k \frac{1}{w} W P_k W^T.$$

Using the sparsity of W in (19), the inverse of the diagonal matrix D is written as

$$D^{-1} = I + \frac{\gamma k}{|D|} \frac{1}{w} W P_k W^T, \quad |D| = 1 - \gamma k w p_{33}. \tag{28}$$

Let us define $\lambda \triangleq \gamma k / |D|$, then the following equation is obtained from (27) and (28).

$$(I - \gamma k P_k W)^{-1} = I + \lambda P_k W \tag{29}$$

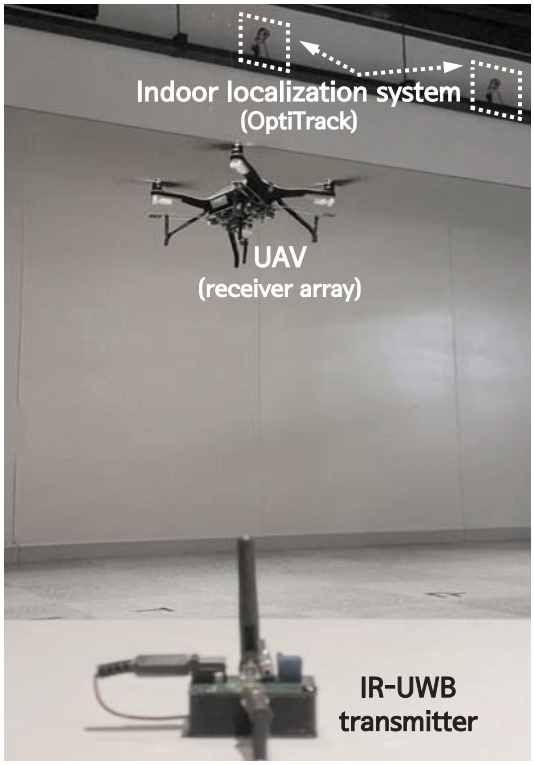

FIGURE 10. Experiment environment.

By substituting (29) into (26), we have

$$\begin{aligned} c(\lambda) &= \hat{\boldsymbol{x}}_k^T (I + \lambda P_k W)^T M (I + \lambda P_k W) \hat{\boldsymbol{x}}_k \\ &= \sum_{m=0}^{2} c_m \lambda^m = 0, \end{aligned} \tag{30}$$

where

$$\begin{aligned} c_0 &= \hat{\boldsymbol{x}}_k^T M \hat{\boldsymbol{x}}_k, \\ c_1 &= \hat{\boldsymbol{x}}_k^T (M P_k W_k + W_k P_k M) \hat{\boldsymbol{x}}_k, \\ c_2 &= \hat{\boldsymbol{x}}_k^T (W_k P_k M P_k W_k) \hat{\boldsymbol{x}}_k. \end{aligned}$$

■

Remark 6: In the case that the equality constraint (25) produces two distinct solutions of γ, we need to choose one of them to compute (17) and (18). For this purpose, it is preferred to choose γ with the smallest absolute value under the assumption that the modeling error is quite small. Since the design parameter W is defined as the weighted sum of the noise variance σ_r^2, a valid solution has to satisfy $\gamma > -1$.

IV. PERFORMANCE EVALUATION

A. CONDITIONS FOR EXPERIMENT

In order to verify the performance of the proposed localization system, simulations and experiments are carried out under the test conditions summarized in TABLE 2. The test results are obtained from 50 Monte-Carlo trials at every test point, depicted in Fig. 4. As in Fig. 2 or Fig. 10, the receiver array is mounted on the HUINS BlueEye-1k UAV.

TABLE 3. Experimental condition.

ITEM	ASSUMPTION
receiver array (UAV)	$\sigma_r^2 = (1.5 \times 10^{-3}[\mathrm{m}])^2$ $d = 0.2$ [m] $(x_0, y_0) = (0, 0)$ [m] $(x_j, y_j) = (x_0, y_0) + d\,(\cos(\psi_j), \sin(\psi_j))$ [m], $\psi_j = \pi/2 \cdot (j-1), \quad j = 1, 2, \cdots, 4.$
initial value	$*$ linear estimator : OWLS, H_∞ filter, RWLS, C-RWLS $P_0 = diag\left(\begin{bmatrix} 20^2 & 20^2 & 2 \cdot 20^2 \end{bmatrix}\right)$ [m^2] $\boldsymbol{x}_0 = 10 \begin{bmatrix} \cos(k\pi/4) & \sin(k\pi/4) & 1 \end{bmatrix}^T + \delta\boldsymbol{x}_0$ [m], $k = \begin{cases} 1, & \text{test point \#1, \#4, \#7} \\ 2, & \text{test point \#2, \#5, \#8} \\ 3, & \text{test point \#3, \#6, \#9} \end{cases}$, $\delta\boldsymbol{x}_0 \sim \mathcal{N}(\mathbf{0},\ P_0/5)$ $*$ non-linear estimator: EKF $P_0^{EKF} = diag\left(\begin{bmatrix} P_0(1,1) & P_0(2,2) \end{bmatrix}\right)$ [m^2] $\boldsymbol{x}_0^{EKF} = \begin{bmatrix} \boldsymbol{x}_0(1) & \boldsymbol{x}_0(2) \end{bmatrix}^T$ [m]

This inspection UAV hovers above each test point while maintaining an altitude of $h = 0.88$ [m]. For the performance analysis, a highly accurate OptiTrack indoor positioning system consisting of 18 Flex13 cameras is used. Using this system, the UAV position with respect to the transmitter can be acquired within 3[mm] accuracy.

The performance of our C-RWLS algorithm is compared with that of a standard RWLS estimator. In addition, we compared the H_∞ filter, which is known as robustness for the parameter uncertainty [24]. The optimal weighted least-squares (OWLS) estimator constituted by the noise-free measurement matrix H_k is also simulated to provide the theoretical performance bound of the linear localization filter. Note that the OWLS estimator cannot be realizable in practice. To show the effectiveness of the linear filter structure for UAV localization using passive measurements, the extended Kalman filter (EKF), which is the most commonly used non-linear localization algorithm, is also considered [25]. Since only the bearing angle can be guessed from the TDOA measurements, the *a priori* position estimate of each localization algorithm is set by using the maximum detection range of our localization sensor, as in TABLE 3. In the table, $\mathcal{N}(m, \sigma^2)$ represents a normal distribution with a mean of m and a variance of σ^2.

B. SIMULATION RESULTS

First, it is checked how the proposed method is useful to guarantee the robustness of the localization filter against the imperfectness of the statistical knowledge on the TDOA measurement noise.

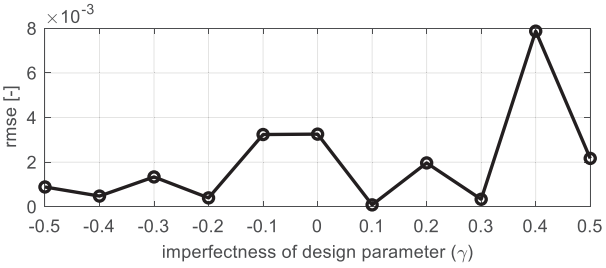

FIGURE 11. Performance of γ calculation: simulation result.

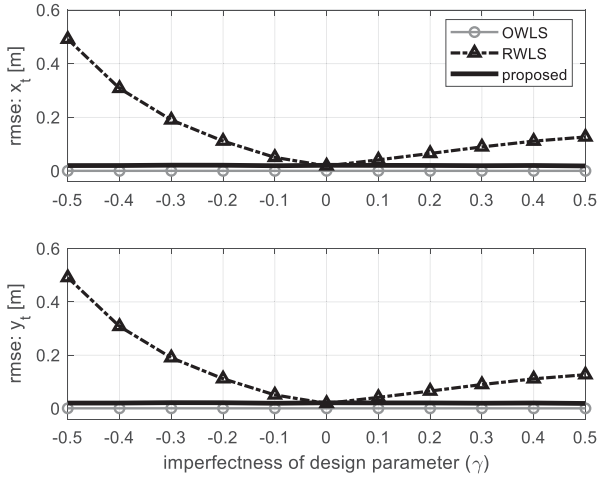

FIGURE 12. Localization performance variation due to the imperfectness of design parameter: simulation result.

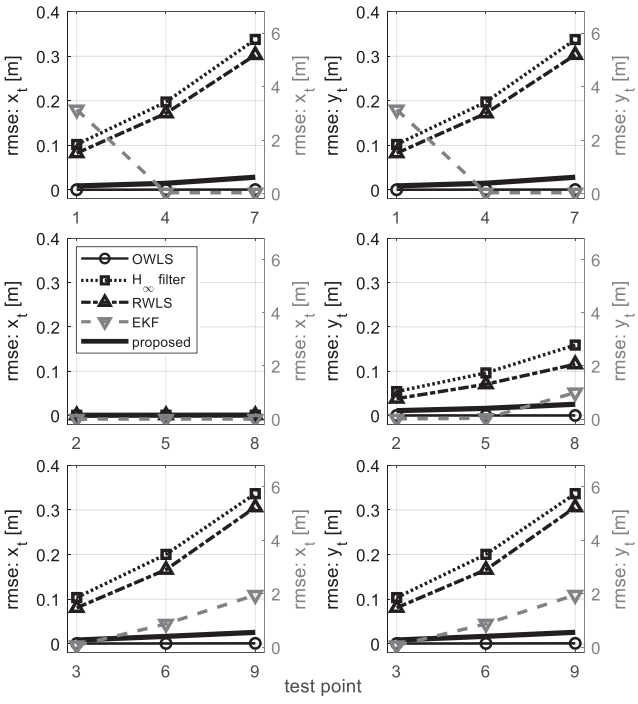

FIGURE 13. Localization performance at various test points: simulation result.

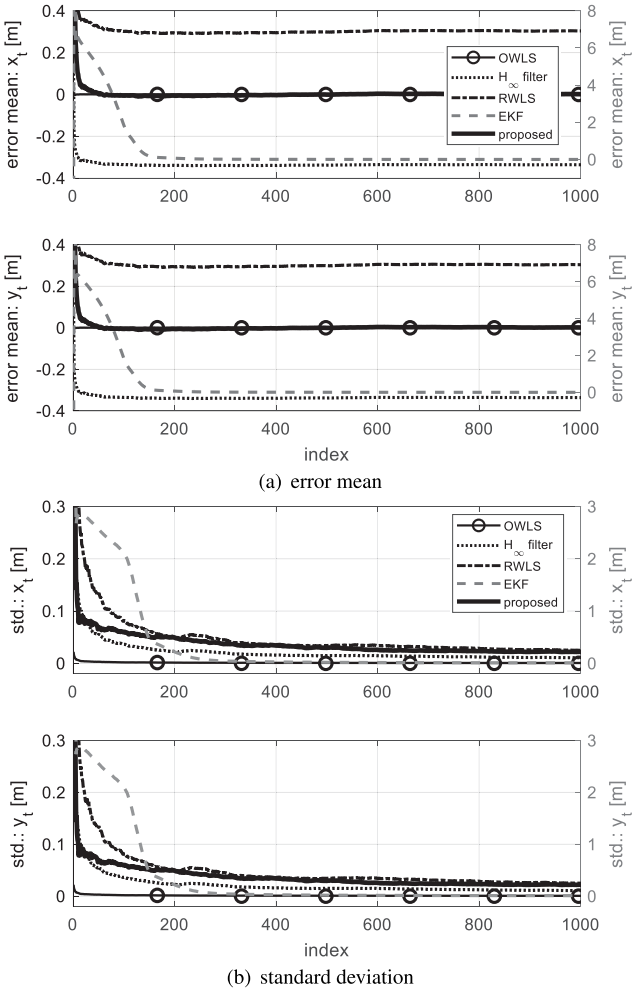

FIGURE 14. Convergence property of localization estimator at test point #7: simulation result.

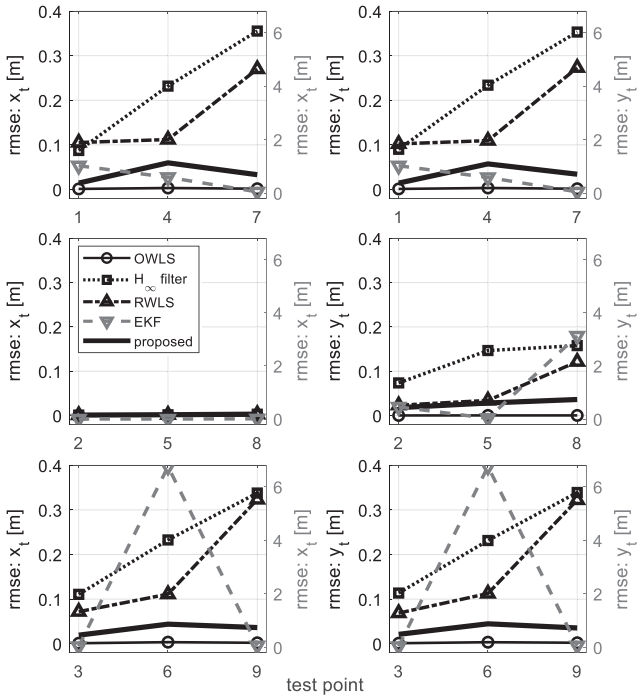

FIGURE 15. Localization performance at various test points: experimental result.

In accordance with the above point, the imperfectness ratio γ is arbitrarily chosen within $-0.5 \leq \gamma \leq 0.5$ and is computed γ by the C-RWLS algorithm. As illustrated in Fig. 11, the root mean square error (RMSE) of γ does not exceed 0.008. It means that the imperfect design parameter W_k is very close to the ideal design parameter W_k^o. So, we can analyze that excellent localization performance is guaranteed even in difficult cases when an accurate design parameter is not computed. Based on this result, it is clear that the imperfectness of the nominal design parameter W_k can be adaptively estimated by ***Theorem 2***.

Also, to discuss the effect of the estimation performance degradation caused by the imperfect design parameter W_k, the RMSE of the localization results toward the compensating parameter γ is depicted in Fig. 12 for the test point #7 in Fig. 4. As the magnitude of the uncertainty of the design parameter γ increases, the performance of the standard RWLS estimator becomes worse and worse. By exploiting the γ compensation algorithm in (25), the C-RWLS estimation scheme produces reliable localization performance even when the ideal design parameter W^o is unknown. In other words, accurate localization could be successfully carried out because it can alleviate the sensitivity problem of the RWLS approach.

Next, the estimation performance when $\gamma = -0.4$ at the every test point in Fig. 4 is shown in Fig. 13. The EKF method has poor estimation performance and does not provide consistent results because of an imprecise initial guess. The RMSE of the H_∞ filter and the RWLS approach does not exceed 0.35[m]. However, one can see that a bias error remains which increases as the distance between the transmitter and the receiver array is far away. Typically, the positioning result from the localization sensor is feedback in the control loop of the UAV to generate a guidance command for a set path. For this reason, if the localization sensor provides a biased estimation error, it might ultimately cause overall performance degradation of the substation inspection UAV. Meanwhile, the proposed C-RWLS localization algorithm, which considers the geometry of the state variables, shows a quasi-optimal estimation performance at every test point. Since it is difficult to model a precise measurement error and its statistics on the stochastic parametric uncertainty in a real substation environment, the proposed estimator may be an excellent choice in such cases.

Furthermore, let us verify the convergence characteristics of each localization performance. The error mean and its standard deviation of the estimators at test point #7 are illustrated in Fig. 14. Due to its inherent nonlinearity, the EKF-based method has a slower convergence rate than linear filters. This implies that a linear estimator structure is

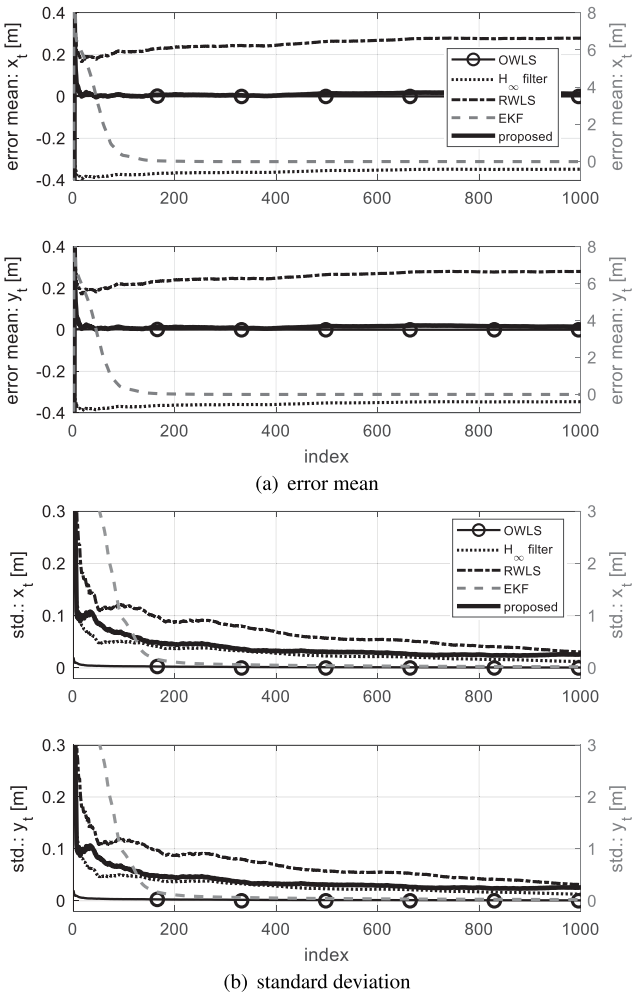

(a) error mean

(b) standard deviation

FIGURE 16. Convergence property of localization estimator at test point #7: experimental result.

advantageous to improve the convergence rate when implementing real-time localization algorithms. Since the H_∞ filter focuses on guaranteeing robustness for parameter uncertainty, conservativeness cannot be avoided. Therefore, a biased error means is still in existence. The standard RWLS method has also a biased error means because of its imperfect design parameter, W_k. On the other hand, the proposed C-RWLS localization estimator increases the error standard deviation by 0.01[m] compared to the H_∞ filter; however, unlike the results of the other algorithms, it satisfies nearly zero-mean characteristics. Thus, the RMSE of the C-RWLS localization algorithm in Fig. 13 shows the closest results to the OWLS estimation result.

C. EXPERIMENTAL RESULTS

To demonstrate the proposed localization system performance, an experiment is performed using the RD measurements obtained from the devised cruciform receiver array in Fig. 2. After equipping the inspection UAV with the devised RD measuring sensor based on the experimental conditions described in Section IV-A, the experiment is executed at the same test point, as Fig. 13 and Fig. 14, and the results are depicted in Fig. 15 and Fig. 16.

The EKF estimates do not satisfy the consistency regardless of the relative geometry between the transceivers, and it converges after the 250th index at test point #7. This is because it cannot know the exact initial value from the characteristics of the passive measurement-based localization method, and it uses the non-linear measurement model. In the case of H_∞ filter and RWLS localization results, its RMSE and convergence characteristics are similar to those of the simulation results. This is because none of these estimation methods can directly deal with the imperfectness of the design parameter W_k modeled as a statistical properties of the RD measurement noise. Whereas, the proposed C-RWLS algorithm meets the RMSE level within 0.05[m] at all test points. Moreover, the proposed approach provides a fast convergence rate and stable estimation performance, despite the use of imperfect design parameter. From the above results, it is expected that the proposed passive localization system can be a viable solution for substation inspection UAVs in non-GPS environments.

V. CONCLUSION

A novel passive localization system was developed for substation inspection UAVs under GPS-denied environments. Firstly, a CMOS IR-UWB-based range difference (RD) measuring sensor was devised. With the help of the passive IR-UWB RD sensor, a high-cost synchronization device between the transceivers was not required. Also, our hardware was significantly less affected by multi-path. Secondly, an uncertain linear measurement model was derived to formulate the UAV localization problem within the framework of linear least-squares estimation theory. Then, a constrained robust weighted least-squares (C-RWLS) estimator was designed to reduce the performance degradation due to the imperfectness of the RD measurement noise statistics that is an important design parameter of the localization algorithm. The geometric relationship between the transmitter and the receiver array was used to correct the erroneous design parameter and to secure the reliability of UAV localization. The effectiveness of our proposed solution for substation inspection UAVs was verified with experimental results.

Our future works aim to check the practicality of the proposed localization system through a performance evaluation in an actual substation or similar environment. In addition, we plan to study a supplemented C-RWLS localization algorithm that can estimate the attitude of inspection UAVs. A plurality of IR-UWB transmitters can be exploited to cope with the performance deterioration of the magnetic sensor mounted on the UAV due to electromagnetic interference in the substation facility.

ACKNOWLEDGMENT

The authors thank Rohde & Schwarz for providing support with the test instruments. The MPW and CAD tools were supported by KAIST IDEC.

REFERENCES

[1] S. Ghosh, D. Ghosh, and D. K. Mohanta, "Situational awareness enhancement of smart grids using intelligent maintenance scheduling of phasor measurement sensors," *IEEE Sensors J.*, vol. 17, no. 23, pp. 7685–7693, Dec. 2017, doi: 10.1109/JSEN.2017.2720779.

[2] S. Kim, D. Kim, S. Jeong, J.-W. Ham, J.-K. Lee, and K.-Y. Oh, "Fault diagnosis of power transmission lines using a UAV-mounted smart inspection system," *IEEE Access*, vol. 8, pp. 149999–150009, 2020, doi: 10.1109/ACCESS.2020.3016213.

[3] S. Jordan, J. Moore, S. Hovet, J. Box, J. Perry, K. Kirsche, D. Lewis, and Z. T. H. Tse, "State-of-the-art technologies for UAV inspections," *IET Radar, Sonar Navigat.*, vol. 12, no. 2, pp. 151–164, 2018, doi: 10.1049/iet-rsn.2017.0251.

[4] Y. J. Ham, K. K. Han, J. J. Lin, and M. Golparvar-Fard, "Visual monitoring of civil infrastructure systems via camera-equipped unmanned aerial vehicles (UAVs): A review of related works," *Vis. Eng.*, vol. 4, no. 1, pp. 1–8, Jan. 2016, doi: 10.1186/s40327-015-0029-z.

[5] T. He, Y. Zeng, and Z. Hu, "Research of multi-rotor UAVs detailed autonomous inspection technology of transmission lines based on route planning," *IEEE Access*, vol. 7, pp. 114955–114965, 2019, doi: 10.1109/ACCESS.2019.2935551.

[6] H. Langaker, H. Kjerkreit, C. L. Syversen, R. J. D. Moore, Ø. H. Holhjem, I. Jensen, A. Morrison, A. A Transeth, G. Berg, O. Kvien, T. A. Olsen, A. Hatlestad, T. Negård, R. Brochand, and J. E. Johnsen, "An autonomous drone-based system for inspection of electrical substations," *Int. J. Adv. Robot. Syst.*, vol. 18, no. 2, pp. 2241–2263, 2021, doi: 10.1177/17298814211002973.

[7] B. Li, Z. Fei, and Y. Zhang, "UAV communications for 5G and beyond: Recent advances and future trends," *IEEE Internet Things J.*, vol. 6, no. 2, pp. 2241–2263, Apr. 2019, doi: 10.1109/JIOT.2018.2887086.

[8] I. Cvišić, J. Ćesić, I. Marković, and I. Petrović, "SOFT-SLAM: Computationally efficient stereo visual simultaneous localization and mapping for autonomous unmanned aerial vehicles," *J. Field Robot.*, vol. 35, pp. 578–595, Jun. 2018, doi: 10.1002/rob.21762.

[9] H. Bavle, P. De La Puente, J. P. How, and P. Campoy, "VPS-SLAM: Visual planar semantic SLAM for aerial robotic systems," *IEEE Access*, vol. 8, pp. 60704–60718, 2020, doi: 10.1109/ACCESS.2020.2983121.

[10] C. Teuliere, E. Marchand, and L. Eck, "3-D model-based tracking for UAV indoor localization," *IEEE Trans. Cybern.*, vol. 45, no. 5, pp. 869–879, May 2015, doi: 10.1109/TCYB.2014.2337652.

[11] J. Wang, J. Huang, and R. Cheng, "Automatic reading system for analog instruments based on computer vision and inspection robot for power plant," in *Proc. 10th Int. Conf. Modelling, Identificat. Control (ICMIC)*, Jul. 2018, pp. 1–6, doi: 10.1109/ICMIC.2018.8529848.

[12] L. Yang, X. Feng, J. Zhang, and X. Shu, "Multi-ray modeling of ultrasonic sensors and application for micro-UAV localization in indoor environments," *Sensors*, vol. 19, no. 8, p. 1770, Apr. 2019, doi: 10.3390/s19081770.

[13] A. Alarifi, A. Al-Salman, M. Alsaleh, A. Alnafessah, S. Al-Hadhrami, M. Al-Ammar, and H. Al-Khalifa, "Ultra wideband indoor positioning technologies: Analysis and recent advances," *Sensors*, vol. 16, no. 5, p. 707, May 2016, doi: 10.3390/s16050707.

[14] F. Lazzari, A. Buffi, P. Nepa, and S. Lazzari, "Numerical investigation of an UWB localization technique for unmanned aerial vehicles in outdoor scenarios," *IEEE Sensors J.*, vol. 17, no. 9, pp. 2896–2903, May 2017, doi: 10.1109/JSEN.2017.2684817.

[15] S. K. Meghani, M. Asif, F. Awin, and K. Tepe, "Empirical based ranging error mitigation in IR-UWB: A fuzzy approach," *IEEE Access*, vol. 7, pp. 33686–33697, 2019, doi: 10.1109/ACCESS.2019.2904201.

[16] O. Jean and A. J. Weiss, "Passive localization and synchronization using arbitrary signals," *IEEE Trans. Signal Process.*, vol. 62, no. 8, pp. 2143–2150, Feb. 2014, doi: 10.1109/TSP.2014.2307281.

[17] U.-S. Suh, Y. Lee, W.-S. Ra, and T. W. Kim, "Robust bearing angle error estimation for mobile robots with a gimballed ultrasonic seeker," *IEEE Trans. Ind. Electron.*, vol. 65, no. 7, pp. 5785–5795, Jul. 2018, doi: 10.1109/TIE.2017.2777411.

[18] U.-S. Suh, T.-W. Kim, D.-H. Kang, K.-M. Lee, W.-S. Ra, and T. Kim, "A robust passive target localization for substation inspection of UAV in a GPS-denied environment," in *Proc. 22nd IEEE Int. Conf. Ind. Technol. (ICIT)*, Mar. 2021, pp. 844–849, doi: 10.1109/ICIT46573.2021.9453470.

[19] L. Stoica, A. Rabbachin, and I. Oppermann, "A low-complexity noncoherent IR-UWB transceiver architecture with TOA estimation," *IEEE Trans. Microw. Theory Techn.*, vol. 54, no. 4, pp. 1637–1646, Jun. 2006, doi: 10.1109/TMTT.2006.872056.

[20] T. H. Jin, H. G. Han, and T. W. Kim, "Time-of-arrival measurement using adaptive CMOS IR-UWB range finder with scalable resolution," *IEEE Trans. Circuits Syst. I, Reg. Papers*, vol. 63, no. 10, pp. 1605–1615, Oct. 2016, doi: 10.1109/TCSI.2016.2583661.

[21] M. Pertijs and J. H. Huijsing, *Precision Temperature Sensors in CMOS Technology*. Springer, 2006.

[22] S. Lu, W. Wang, and G. Wang, "Stationary points of a kurtosis maximization criterion for noisy blind source extraction," *IEEE Access*, vol. 5, pp. 8736–8740, 2017, doi: 10.1109/ACCESS.2017.2703840.

[23] T. Liu, F. Wen, L. Zhang, and K. Wang, "Off-grid DOA estimation for colocated MIMO radar via reduced-complexity sparse Bayesian learning," *IEEE Access*, vol. 7, pp. 99907–99916, 2019, doi: 10.1109/ACCESS.2019.2930531.

[24] D. Simon, *Optimal State Estimation: Kalman, H Infinity, and Nonlinear Approaches*. Hoboken, NJ, USA: Wiley, 2006.

[25] R. Zhang, F. Höflinger, and L. Reindl, "TDOA-based localization using interacting multiple model estimator and ultrasonic transmitter/receiver," *IEEE Trans. Instrum. Meas.*, vol. 62, no. 8, pp. 2205–2214, Aug. 2013, doi: 10.1109/TIM.2013.2256713.

UI-SUK SUH received the B.S. and M.S. degrees in mechanical and control engineering from Handong Global University, Pohang, South Korea, in 2015 and 2017, respectively, where he is currently pursuing the Ph.D. degree with the School of Mechanical and Control Engineering. He is also currently pursuing the Ph.D. degree in electrical and electronic engineering with Yonsei University, Seoul, South Korea. Since December 2022, he has been with the Maritime Technology Research Institute, Agency for Defense Development, Changwon, South Korea, as a Researcher. His research interests include automatic target recognition, information fusion filter, autonomous vehicle control, and related sensor technology.

GEUNHAENG LEE was born in Seoul, South Korea, in 1991. He received the B.S. degree in electronic and electrical engineering from Dankook University, Yong-in, Kyung-ki, South Korea, in 2014, and the Ph.D. degree in electrical and electronic engineering from Yonsei University, Seoul, in 2021. He was with System LSI Business, Samsung Electronics, Hwaseong, South Korea, from 2021 to 2023, as a Staff Engineer, where he was involved with design of UWB RF transceiver (IEEE 802.15.4z). Since March 2023, he has been with the Department of Electronic Engineering, Andong National University, as an Assistant Professor. His research interests include RF amplifiers including PA and LNA, mixed-signal circuits, circuit and system for wireless communication, UWB transceiver systems, mm-wave ICs, and digital transmitter.

JIEUN HAN received the B.S. degree in mechanical and control engineering from Handong Global University, Pohang, South Korea, in 2021, where she is currently pursuing the M.S. degree in mechanical and control engineering. Her research interests include guidance and control, including its application to autonomous systems.

TAE WOOK KIM (Senior Member, IEEE) was born in Seoul, South Korea, in 1974. He received the B.S. degree in electrical engineering from Yonsei University, Seoul, in 2000, and the M.S. and Ph.D. degrees from the Korea Advanced Institute of Science and Technology (KAIST), Daejeon, South Korea, in 2002 and 2005, respectively. He was with Qualcomm Inc., Austin, TX, USA, where he was involved with DVB-H and media FLO chip design. Since September 2007, he has been with the School of Electrical and Electronic Engineering, Yonsei University, where he is currently a Professor. His research interests include microwave, RF, analog, and mixed-signal ICs and systems. He was served as a Technical Program Committee Member for IEEE ISSCC, IEEE A-SSCC, and IEEE APMC, and an Organizing Committee Member of IEEE A-SSCC. He is serving as a TPC Member for IEEE RFIC and a Steering Committee Member for IEEE MWSCAS.

WON-SANG RA received the B.S. degree in electrical engineering, the M.S. degree in electrical and computer engineering, and the Ph.D. degree in electrical and electronic engineering from Yonsei University, Seoul, South Korea, in 1998, 2000, and 2009, respectively. From March 2000 to February 2009, he was with the Guidance and Control Department, Agency for Defense Development, Daejeon, South Korea, as a Senior Researcher. Since 2009, he has been with the School of Mechanical and Control Engineering, Handong Global University, Pohang, South Korea, where he is currently a Professor. Since 2015, he has been collaborating with the School of Aerospace, Transport, and Manufacturing, Cranfield University, U.K., as a Visiting Professor. His research interests include the filtering theory and its application to radar target tracking, distributed sensor fusion, and autonomous vehicle guidance.